 doi:10.20944/preprints202101.0357.v1

Article

Using GRACE/GRACE-FO, Data-Driven, and Modeling to Assess the Twentieth and Twenty-first Century Water Storage Changes in the Nile River Basin

Emad Hasan[1,6*], Aondover Tarhule[2] and Pierre-Emmanuel Kirstetter[3,4,5]

[1] Department of Geological Sciences and Environmental Studies, State University of New York, SUNY at Binghamton, NY, USA; emad.hasan@binghamton.edu
[2] Department of Geography, Geology, and the Environment, Illinois State University, Normal, IL, USA; tarhule@ilstu.edu
[3] School of Meteorology, University of Oklahoma, Norman, OK; pierre.kirstetter@noaa.gov
[4] School of Civil Engineering and Environmental Science, University of Oklahoma, Norman, OK
[5] NOAA/National Severe Storms Laboratory, Norman, OK
[6] Geology Department, Faculty of Science, Damietta University, New Damietta, Egypt
* Correspondence: emad.hasan@binghamton.edu

Abstract: This research assesses the changes in the total water storage (TWS) during the twentieth century and their future projections in the Nile River Basin (NRB) via TWSA (TWS anomalies) records from GRACE (Gravity Recovery and Climate Experiment), GRACE-FO (Follow-On), data-driven-reanalysis TWSA and land surface model (LSM), in association with precipitation, temperature records, and standard drought indicators. The analytical approach incorporates the development of 100+ yearlong TWSA records using a probabilistic conditional distribution fitting approach by the GAMLSS (Generalized Additive Model for Location, Scale, and Shape) model. The drought and flooding severity, duration, magnitude, frequencies, and recurrence were assessed during the studied period. The results showed, 1- The NRB between 2002 to 2020 has transited to substantial wetter conditions. 2- The TWSA reanalysis records between 1901 to 2002 revealed that the NRB had experienced a positive increase in TWS during the wet and dry seasons. 3- The projected TWSA between 2021 to 2050 indicated slight positive changes in TWSA during the rainy seasons. The analysis of drought and flooding frequencies between 1901 to 2050 indicated the NRB has ~64 dry-years compared to ~86 wet-years. The 100+ yearlong TWSA records assured that the NRB transited to wetter conditions relative to few dry spells. These TWSA trajectories call for further water resources planning in the region especially during flood seasons. This research contributes to the ongoing efforts to improve the TWSA assessment and its associated dynamics for transboundary river basins. It also demonstrates how an extended TWSA record provides unique insights for water resources management in the NRB and similar regions.

Keywords: GRACE; GRACE-FO; TWS; hydroclimatic; drought; flooding; Nile River Basin; Africa

1. Introduction

The Nile river basin (NRB; ~3.18 million Km^2) is a complex transboundary hydrologic system [1-4], and one of the world's preeminent geopolitical hotspots [5-8]. The NRB is home to more than 320 million people belonging to 11 African nations (2018 population estimation), approximately 24 percent of Africa's total population [9, 10]. To both upstream and downstream countries, the Nile river is crucial for development planning, food, and energy productions. Egypt, a major downstream country, depends on the Nile River for its survival more completely than any other country depends on any single waterway [11]. Yet, the water flowing in the Nile originates entirely outside Egypt's borders. To the other 10 other countries, the Nile water is critically needed for energy generation,

 doi:10.20944/preprints202101.0357.v1

to assure their own food security, mitigate the disastrous effects of periodic droughts, and assure social-economic development [5, 12, 13].

Consequently, from the point of view of hydropolitics and hydroclimatology, the NRB is also one of the most intensely studied and researched basins in the world. Specifically, considerable effort has focused on modeling the flow dynamics of the basin [14-19], water balance [20-23], groundwater [24-26], and precipitation variability [27, 28] among numerous others. Despite the plethora of existing studies, recent data acquisition methods and algorithmic solutions afforded by platforms such as GRACE (Gravity Recovery and Climate Experiment) and GRACE-FO (Follow-On) satellite data have begun to produce additional insights into the dynamics of water resources in the NRB [22, 29-34]. GRACE-derived TWSA (total water storage anomalies) data integrate storage changes in all forms of water, including surface water storage (SWS), soil moisture storage (SMS), groundwater storage (GWS), and snow water equivalent (SWE), as well as the impacts of anthropogenic processes on these stocks of waters [35-38]. Significantly, therefore, the spatial and temporal patterns of TWSA produced by GRACE are unique and distinct from those generated by other sources, such as Land Surface Models (LSMs) outputs and hydrologic model [39, 40].

The new and unique perspectives produced by GRACE point to a need for the application of the same consistent methodology in the pre-GRACE period. Herein, we report a reconstruction of monthly TWSA data for the Nile Basin spanning the entire 20th century. To achieve the reconstruction, we integrated the current GRACE TWSA observations, with probabilistic simulated TWS records (see section 3.5) for past scenarios to provide an overview of the TWSA variability in the NRB. Armed with the new 100 yearlong TWSA simulated time series, we investigated several hydroclimatic dynamics in the NRB, including floods, droughts, and spatiotemporal water storage variability across the basin. Additionally, we used the same analytic framework to generate future projections of TWSA for the period 2021 to 2050. In total, therefore, our approach allowed us to extend the TWS data both backward (by 80 years) and forward (by 30 years) using the same consistent data and methodology. The reconstructed/projected GRACE data reproduced many established hydroclimatic events in the NRB based on other independent data types, including floods, droughts, and periods of wet and dry regimes. The results also point to important differences between new estimates generated using GRACE data compared to those produced from other data types.

As noted previously, the NRB has been intensively studied both in terms of historical and future trends of runoff and precipitation. For instance, the runoff vulnerability in the NRB to climate change was assessed using streamflow records [17], hydrological model outputs [28], and projected precipitation, and temperature records [18, 41, 42]. The precipitation, evapotranspiration (ET), and Potential ET (PET) were utilized to assess the runoff variability to future climate projections in the basin [18]. Other research studies assessed the water budget in the basin using lumped records of GRACE-TWSA as well as multisource remote sensing observations across the NRB, and individual hydrologic units, i.e., Lake Victoria [23, 43], Blue Nile Basin (BNB) [16, 44, 45]. Besides, the GRACE TWSA variability in the NRB was analyzed over "space" relative to different hydroclimatic and anthropogenic processes between 2002 to 2016 [29].

None of the available/previous research, however, has provided a comprehensive evaluation of the TWSA, especially through the past century. Nevertheless, none has provided a foreseen evaluation of the TWSA changes to assess the enduring anthropogenic activities on the Nile waters. Yet, the most recent record of GRACE-FO TWSA is not fully implemented to assess the most recent variability across the basin. This paper, therefore, is a contribution to ongoing efforts to improve the assessment of the TWSA and its associated dynamics in the NRB. The presented results have theoretical and practical

Preprints (www.preprints.org) | NOT PEER-REVIEWED | Posted: 18 January 2021 doi:10.20944/preprints202101.0357.v1

applications related to the management of the basin's shared and transboundary water resources. The mismanagement of the water storage in the NRB, therefore, would amplify additional instability context and would transit the basin to unrest hydro-conflict hotspot for food, water, and energy quest. Understanding the TWS changes is critical to, (i) scheme best management practice for the basin's available water resources, (ii) identify the potential TWS trajectories that would sustain future hydropower management plans.

2. The Nile River Basin (NRB)

With a total flow length of 6850 Km long, the Nile is the world's longest river and the second (after the Amazon) in terms of the watershed area. Unique among African rivers, the Nile flows from south to north as a confluence of two rivers, the White Nile and the Blue Nile rivers. Annually, the average natural water flow in the Nile generates a total runoff estimated at approximately 88 ±5 BCM/yr. (Billion Cubic Meter) at Aswan High Dam in Egypt. In general, the Nile basin can be divided into four major sub-basins [1]: (1) The White Nile Basin (WNB); (2) The BNB; (3) The Atbara River Basin; and (4) The Main or trunk stem Nile Basin. Within the WNB, the Nile takes its rise from the Equatorial Lake system (Lake Victoria water tower in the south). Northward, the river flows into the Sudd wetlands, spreading across nearly 57,000 km2 and markedly slowing down. As a result, approximately 4 BCM of water are lost to evaporation here making the Sudd the main water sink region in the WNB. As a result of these losses, the White Nile, which 37 BCM/yr. near its source produces only 33 BCM/yr. or 29 percent of the total Nile runoff downstream of the Sudd. The Blue Nile River originates at Lake Tana in the Ethiopian highlands. It generates about 57 percent (50.6 BCM/yr.) of the total runoff to the Nile. The Atbara River rises in northern Ethiopia. It is a flashy river that is dry for half the year. The Atbara contributes ~14 percent (4.4. BCM/yr.) of the total Nile runoff. The Main Nile Basin begins at the confluence of the White and Blue Niles. It also receives flow from the Atbara River a short way downstream. The Main Nile Basin itself grades from semiarid to arid in the north. Consequently, the basin experiences little to no surface runoff. It also experiences large evaporation losses due to high temperatures nearly year-round [6], 2000), the Main Nile is the second water sink region in the basin (Figure 1).

Total annual rainfall is variable in amount and timing across the different sub-basins of the NRB. In the Equatorial Lakes, the rainfall varies between ~900 to 2000 mm/yr. The rainy season is bimodal, occurring between March to May and August to December [2].

The Ethiopian highlands receive annual varies between 1200 and 1800 mm/yr. with an average of about 1000 mm/yr. Most precipitation occurs between July to October. For the Atbara sub-basin, the annual average precipitation reaches 553 mm/yr., the lowest among other southern Nile sub-basins [9]. The rainfall amount over Sudd wetlands is around 800 to 900 mm/yr., occurring from April to November [46]. The precipitation rate across the Main Nile Trunk, located within the arid climates, is approximately 200 mm/yr. [9].

As a product of precipitation (gross precipitation rates), theoretically, the basin's water storage would reach ~1661BCM/yr. The sole contribution of each water source in the basin is as follows, the Equatorial Lakes would provide ~517 BCM/yr., the water storage at the Ethiopian highlands would reach ~ 935 BCM/yr. and only ~590 BCM /yr. of which reaches the Blue Nile waters; At southern Sudan, the total storage reaches ~ 554 BCM/yr. to the Nile water. The total precipitation flux within the basin would produce an average of 1000 m3/yr. per capita; an amount that would surpass the present absolute water scarcity status; the available Nile water shares per capita is less than ~ 500 m3/yr. [13, 47]. Several climate projections revealed a spike in the rainfall amount in the NRB [42, 48]. Despite these projections, the hot and dry conditions coupled with a rising population will reduce the amount of runoff and the water available for agricultural, ecological, and residential use [48].

Preprints (www.preprints.org) | NOT PEER-REVIEWED | Posted: 18 January 2021 doi:10.20944/preprints202101.0357.v1

Due to terrain-topography and climate complexities, the river flow is significantly low, ~0.98 L/s. Km2 or ~99.20 BCM/yr. [25, 45, 49]; the Nile river is one of the lowest flowing rivers globally. The total runoff waters in the Nile river basin are assessed at 161 BCM annually, with total waters reached to Aswan in Egypt ~84 BCM/yr., which is less than 5 percent of the total drainable waters' storage in the basin; ~54 km3 per annum arriving at the delta [50]. The runoff is a key component of the water balance that defined the amount of renewable water resources within the basin [50]. The lack of in situ and gauging stations in the region made such assessment incomprehensive and fragmented; few gauge stations are available to monitor the total streamflow, on the main Blue Nile watercourse, at the headwater zone at Owen reservoir, at the exists of White Nile, Atbara tributaries, and as cumulative streamflow from all tributaries at Aswan Dam (see Figure 1).

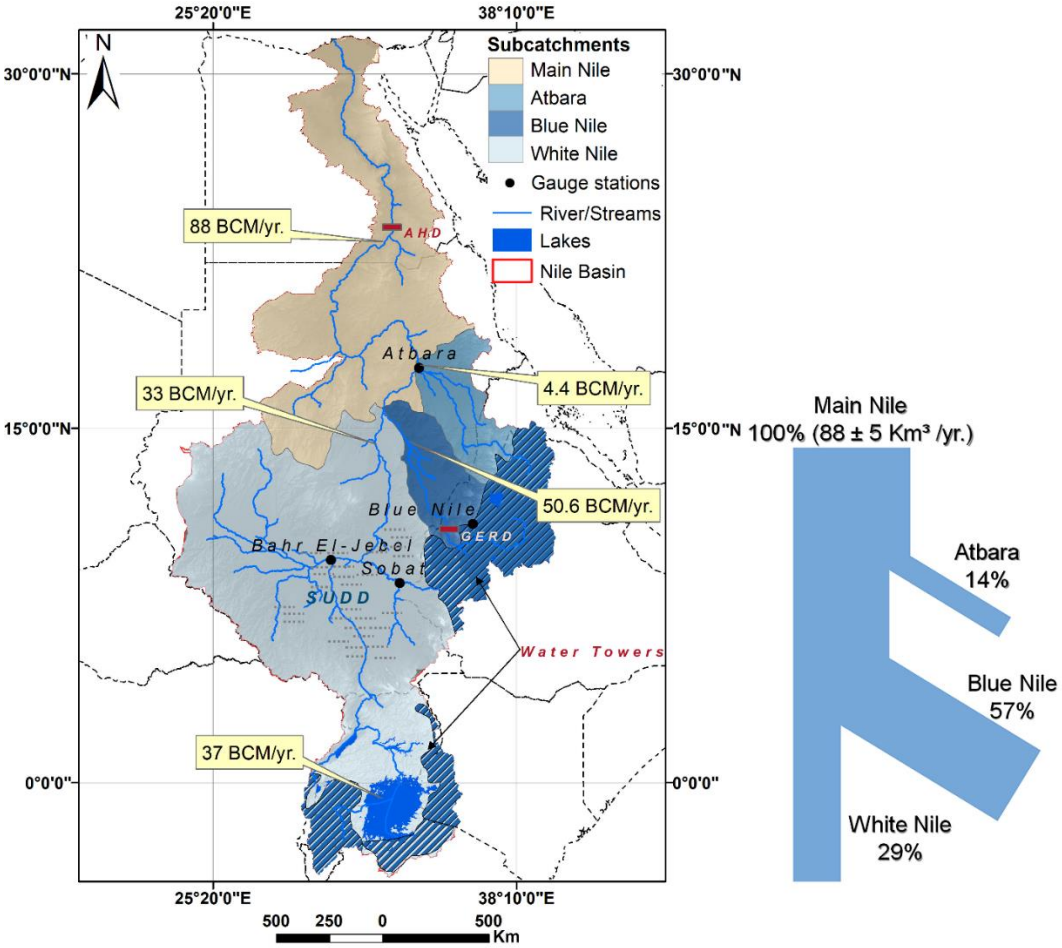

Figure 1. The annual contribution of the major tributaries to the NRB waters; The storage values are an approximation to the annual discharge figures. Source after [51].

The Actual ET figures follow the general precipitation patterns across the basin, where ET rates exceed 1000 mm/yr. in the Equatorial Lake region, and drop to less than 80 mm/yr. in the arid zone [3, 27, 52]. Higher ET rates across the region are responsible for significant water loss annually. The ET diminished ~260 to 310 BCM of water over the Equatorial lakes, Lake Tana and Sudd marshes, ~7 BCM at the conjunction of the two river systems, and ~19 BCM yearly over the Lake Nasser area [53]; in total ~286 to 336 BCM water loss to ET yearly. The basin, resides several natural Lake systems, open water areas, and artificial reservoirs that provide a buffer against seasonal rainfall variations, and maintain a regular water flow; The total lakes area, however, represents less than 3 percent of the basin's total area.

 doi:10.20944/preprints202101.0357.v1

3. Data and Methods

This research utilizes several gridded observations for hydrological variables (i.e., TWSA, precipitation), temperature estimates, and a number of drought indicators. The datasets were available at various grid-scales and spanned different temporal extents. To reconcile with the varied spatial resolutions, the data were summarized at the same spatial extent, either for the basin-level or the sub-basin scale.

3.1. GRACE data

GRACE and GRACE-FO (Follow-On) missions provide an excellent source of global TWSA [38]. GRACE expresses the TWSA as Equivalent Water Thickness (EWT) variation in cm/month. Arithmetically, GRACE TWSA is the sum of changes in water stored in all forms i.e.,

$$\Delta TWS = \Delta SWS + \Delta SMS + \Delta GWS + \Delta SNS \quad (1)$$

where, ΔSWS represents changes in surface water storage; ΔSMS represents changes in soil moisture storage (SMS); ΔGWS represents changes in groundwater storage, and ΔSNS represents changes in snow cover.

GRACE TWSA estimates are available either as spherical harmonic (SH) and or mass concentration blocks (mascon) solutions [54-57]. Three major mission partners produce these estimates namely; the Center for Space Research, University of Texas Austin (CSR; SH and mascon), the Jet Propulsion Laboratory in California (JPL; SH and mascon), and the Geo Forschungs Zentrum (GFZ, SH) in Potsdam, Germany. GRACE TWSA records are available between 2002 to 2017, and the GRACE-FO TWSA data covers the period between 2018-2020. This research utilized the most recently released GRACE and GRACE-FO SHs and mascons of version 2, release- 6 (RL06)

3.2. Land surface model (LSM)

TWS estimates were also extracted using Land surface model (LSM) outputs. In this research, storage estimates were derived from GLDAS (Global Land Data Assimilation System) LSM versions, GLDAS 2.2 of CLSM-F2.5. The GLDAS data were obtained from the GSFC Hydrological Sciences Laboratory (HSL) and the Goddard Earth Sciences Data and Information Services Center (GES DISC). The data are available at 0.25° × 0.25° grid resolution for the period between 1948 and 2014.

3.3. GPCC and CRU datasets

We utilized long-term precipitation records between 1901-2020 from the GPCC (Global Precipitation Climatology Centre) gridded gauge-analysis precipitation products. The data were obtained from the Deutscher Wetterdienst (DWD), the German Meteorological Service. The GPCC provides global monthly gauge-corrected precipitation products at 0.5° x 0.5° grid-scale [58, 59]. The long-term monthly precipitation, temperature, and PET records were obtained from the CRU (Climate Research Unit) at the University of East Anglia, UK, time-series (TS) datasets. The CRU data were calculated at a resolution of 0.5°x0.5° based on 4000+ weather stations around the world [60]. This research employed the most recently released CRU-TS of version 4.04 between 1901- 2020.

The future precipitation and temperature projections were obtained using the CRU ClimGen precipitation and temperature records between 2021 to 2050. The datasets are freely available through the CRU ClimGen data portal. The ClimGen datasets provide spatial climate scenarios for future climate records at regional scales [61]. ClimGen is based on the "pattern-scaling" approach, which encompasses the geographical, seasonal, and multi-variable structure of future climate information. The ClimGen was simulated by coupled atmosphere-ocean general circulation models (AOGCMs) under different

Preprints (www.preprints.org) | NOT PEER-REVIEWED | Posted: 18 January 2021 doi:10.20944/preprints202101.0357.v1

emission scenarios. ClimGen provides these scenarios in a common format, with options to extract user-defined regions, seasons, and specific periods. For more information about the ClimGen data please see [61]

3.4. Drought indicators

To characterize different drought incidents across the NRB region, several drought indicators were employed including the GPCC drought index (GPCC_DI) between 1952 to 2014 [62]; the CRU self-calibrated Palmer Drought Severity Index (scPDSI) between 1901 to 2018; Palmer Drought Severity Index (PDSI) 1901 to 2014; the Standardized Precipitation Index (SPI) between 1901 to 2016; the Standardized Precipitation-Evapotranspiration Index (SPEI) between 1901 to 2015 [63]. The SPI and SPEI were utilized on 6-moths time scales. The scPDSI was determined using the CRU precipitation and PET records according to the scPDSI-package in R Development [64]; the SPI was calculated using precipitation records according to [65]. Table S1 provides the source links and information about the rest of the utilized drought indicators in this research. Additionally, the long-term drought records were constructed for the period between 1901- 2050 using the GRACE-based total water storage deficit (TWSD), and extended TWSD indicators, (see section 3.9).

3.5. GAMLSS model

To develop retrogressive (inclusive) TWSA records for the NRB between 1901-2002, and projected (exclusive) TWSA records from 2021 to 2050, a probabilistic conditional distribution fitting was performed using the GAMLSS (Generalized Additive Model for Location, Scale, and Shape approach) model [66]. The long-term CRU precipitation and temperature records were used as regressors to estimate TWSA, the predictand. The GAMLSS approach makes use of a probability distribution function (PDF) scheme to accommodate the nonlinearity between the predicted and predictor variables as well as in the location and heteroskedasticity in scale.

The model was developed using the monthly TWSA records between 2002-2010 as a training period and subsequently validated using the TWSA data from 2011-2017. The assumption is made that the training TWSA set between 2002-2010 follows known distribution with density f (TWSA|μ,σ) conditional on the parameters mean (μ), and standard deviation (σ). Similarly, the mutually independent observed TWSA records for 2011-2017 give the parameter vector (μ,σ). Simply, to distinguish between systematic variability/trend and (random) uncertainties, conditional PDFs are fitted using the first two moments: the location, μ, describing the systematic trends, and the scale, σ, representing the associated uncertainties. The distribution was given according to Equation 2 as,

$$f(TWSA|\mu,\sigma) = \frac{1}{\sqrt{2\pi}\sigma}\, e^{-\frac{(TWSA-\mu)^2}{2\sigma^2}} \quad (2)$$

After selecting the distribution family, an iterative procedure following forward, backward, and step-wise models were used to refine the model structure and to test the best model output. Then, penalized splines are used to fit the trends for each parameter for their flexibility to model complex nonlinear relationships [67, 68]. The GAMLSS goodness-of-fit was tested using supervised diagnostic plots and significant information criteria test (i.e., the Akaike Information Criterion (AIC), the Schwarz Bayesian Criterion (SBC), the generalized AIC), as well as standard goodness-of-fit diagnostics. Based on the model performance during the training and validation periods, the GAMLSS model is used to build the backward (retrogressive) inclusive records for TWSA between 1901-2002, and forward exclusive TWSA records from 2021 to 2050. Additionally, the GMLSS model provides a set of probabilistic quantile ranges (Q), from Q05 to Q95, within it all possible TWSA is generated. For additional details about the GAMLSS model, please see [68]. The model was accessed using the GAMLSS-package in R Development [69].

Preprints (www.preprints.org) | NOT PEER-REVIEWED | Posted: 18 January 2021 doi:10.20944/preprints202101.0357.v1

3.6. ARIMA model

To fill the one-year gap (July 2017 to July 2018) between GRACE and GRACE-FO records, an ARIMA (Auto-Regressive Integrated Moving Average) model was performed on GRACE TWSA data. The ARIMA was selected to explore another statistical-based approach (deterministic statistic) to fill the missing record between GRACE and GRACE-FO. The ARIMA model generates a single output predication of the input variable using the variable main statistical characteristics, moving average, autocorrelation, seasonal, and different lags. The model follows a system of linear equations to capture the relationship between two consecutive values of the system as:

$$Y_t = \sum_{i=1}^{p} a_i Y_{t-i} + \sum_{i=1}^{q} m_i \, \varepsilon_{t-i} + \varepsilon_t \quad (3)$$

where, Y_t is the independent variable. The missing value is derived using the variables first differencing of Y_{t-i} and the (p, q), which represent the variable autoregressive and moving average parameters respectively. The terms (a_i, m_i) represent the model coefficient for the seasonal and moving average, the error term is given as (ε_t), and is generally assumed to be independent and randomly distributed. The ARIMA model non-seasonal part of the ARIMA model is set at 0-order, 1-degree of differencing, and the 1-month moving average. The seasonal part of the model is fixed using the same parameters' set with a seasonal spike at lag 12. The model was accessed using the forecast-package in R Development [70]. The model's goodness-of-fit was tested using the AIC criterion among other criteria.

3.7. Uncertainty analysis and model performance

The uncertainty in GRACE-TWSA and LSM-based TWSA were assessed following a standardized approach introduced by [71, 72]. Specifically, each time series was detrended by removing the deterministic components (long-term trend). The annual and semi-annual components were removed using STL (seasonal and trend decomposition using LOESS decomposition model as,

$$S_{total} = S_{cycle\ trend} + S_{seasonal} + S_{residual} \quad (4)$$

where, S_{total} the total time series component, $S_{cycle\ trend}$ the cycle/cyclic trend, $S_{seasonal}$ Seasonal component, $S_{residual}$ residual component.

Next, a linear regression approach was applied to remove any further trend signals in the reminder signals (residual), then we interpreted the standard deviation as the maximum uncertainty or measurement error (the amplitude of the measurement error). This approach was utilized to express the uncertainty bounds for the retrogressive and the projected TWSA records as well.

The CRU precipitation data were evaluated against the GPCC gauge corrected precipitation record. GAMLESS and ARIMA models' performances were tested using standardized evaluation criteria including, coevolution between simulated and actual TWSA via cumulative distribution function (CDF), Pearson correlation coefficient (R-Square), the Nash Sutcliffe efficiency (NSE), Root Mean Square Error (RMSE), in addition to other goodness-of-fit coefficients. The performance of the GAMLSS-based long-term TWSA, GRACE-based TWSD was evaluated using LSM-based TWSA and standardized drought indicators.

3.8. NRB Water Storage

The water storage was assessed using an ensemble record of SH and mascons solutions between 2002 to 2020 for the NRB, two major water source areas (i.e., Lake Victoria and BNB water towers), and two main water sink regions (Sudd basin and Main Nile

Preprints (www.preprints.org) | NOT PEER-REVIEWED | Posted: 18 January 2021 doi:10.20944/preprints202101.0357.v1

area). The analysis over the water towers and water sinks was carried out at the mascon levels of 3°×3° degree area. The missing GRACE record between July 2017 to July 2018 was estimated using the ARIMA approach, see section 3.6. The storage assessment was done for wet periods between July to October, and dry periods from November to June for the NRB, BNB, and Sudd basin. Because of a two-month storage lag, the wet period for the Main Nile area runs between September to December, and the dry period goes from January to August. Because the Lake Victoria water tower region is characterized by bimodal wet periods between March to May and August to December, the intervening months define the dry period in the region. CLSM-F2.5 LSM-based TWSA estimates were used to assess comparative TWSA estimates for the NRB.

Additionally, the STL approach (Equation 4) was utilized to assess the TWS annual cycle trends over the NRB. Next, to identify the relative changes in the mean (short-term average) TWSA water storage, a regime-shift detection (change in the mean) was applied on the total TWSA time series and cycle component; The regime-shift algorithm was developed by [73].

3.9. GRACE Total Water Storage Deficit (TWSD)

GRACE-based total water storage deficit (TWSD), and extended TWSD were calculated by comparing the monthly TWSA to a reference monthly value. Herein we utilized the monthly median value for time series data as,

$$TWSD_i = TWSA_i - M \quad (5)$$

where, $TWSD_i$ is the water storage deficit for the i month, TWS_i is the corresponding monthly TWSA, and M is the median value. GRACE-TWDS or drought severity index (DSI) defines the drought and flooding incidents across the season.

Then, the drought severity levels were obtained via standardizing the TWSD values as follows,

$$sTWSD_i = \frac{TWSD_i - \overline{TWSD}}{\sigma} \quad (6)$$

where, $\overline{TWSD}$ is the mean TWSD value, and σ is the standard deviation.

The sTWSD delineates the conditions from very dry to very wet following standard thresholds, see supplementary info Table S2. Similarly, we standardized all drought indicators utilized in this research following Equation 6.

To assess the year-to-year flooding and drought frequencies in the NRB, the severity, timing, and duration of each event were assessed. Severity was described as extreme wet – normal – and extreme dry using standardized indicators. Likewise, to assess the exceedance probability, and recurrence, each flood event was ranked according to the severity levels. The exceedance probability was then calculated as,

$$E = \frac{R}{n-1} \quad (7)$$

where R is the rank, n is the total number of years on record.
The recurrence (return period) was calculated as,

$$RI = \frac{1}{E} \quad (8)$$

The timing and duration were assessed by the approximate dates of onset and cessation, the accumulated magnitude during the incident as,

Preprints (www.preprints.org) | NOT PEER-REVIEWED | Posted: 18 January 2021 doi:10.20944/preprints202101.0357.v1

$$DM = -\{\sum_{j=1}^{x} X\} \quad (9)$$

4. Results

4.1. Present TWS changes in NRB (2002 to 2020)

Figure 2 shows the basin-wide TWSA time series between 2002 to 2020 from GRACE, ARIMA, and GRACE-FO. The result of homogeneity and change-point analysis (Figure 2A), revealed four periods of positive storage increase and two periods of negative decreases. Notably, two consecutive periods of increases since 2012 have raised the average TWSA fivefold relative to the early part of the series. Explicitly, 1- between April 2002 to January 2003, the mean average TWSA pinned at ~33 Gt./yr., 2- between August 2006 to January 2008, ~58 Gt./yr. of storage with ~75 percent increase in the storage, 3- the period between July 2013 to July 2019 during which mean storage increased to 86 Gt./yr. or ~ 48 percent increase relative to the previous period. 4- Between August 2019 to June 2020, the mean annual storage in the NRB reached the highest storage of ~280 Gt./yr. or more than a 2-times increase relative to the storage levels between 2013 to 2019. On the other hand, the TWSA record between 2002 to 2020 indicates two periods of storage reduction, between February 2004 to July 2006, the storage dropped ~–58 Gt./yr. In the second period between February 2009 to June 2012, the storage loss levels reached ~–24 Gt./yr. or ~ 1.4 times recovery levels in the storage losses compared to the previous period. The TWSA cycle trend component, Figure 2B, exhibits 6 main wet cycles; the wet cycles exhibit a significant TWSA storage increase from ~45 Gt./yr. between April 2002 to April 2004 to ~251 Gt./yr. in the late year, 2019 or ~ 8.5 times increase in the wetness levels during the year from June 2019 to June 2020. The TWSA cycle showed three negative cycles, where storage losses started at ~ –41 Gt./yr. between April 2004 to October 2010, then ~–42 Gt./yr. between December 2008 to June 2012, to finally ~–35 Gt//yr. between October 2016 to June 2017. The TWSA cycle indicates ~ 17 percent in storage recovery between 2004 to 2016. Table S3 and Table S4 in the supplementary info summarize the wet and dry records between total TWSA time series and cycle components.

Preprints (www.preprints.org) | NOT PEER-REVIEWED | Posted: 18 January 2021 doi:10.20944/preprints202101.0357.v1

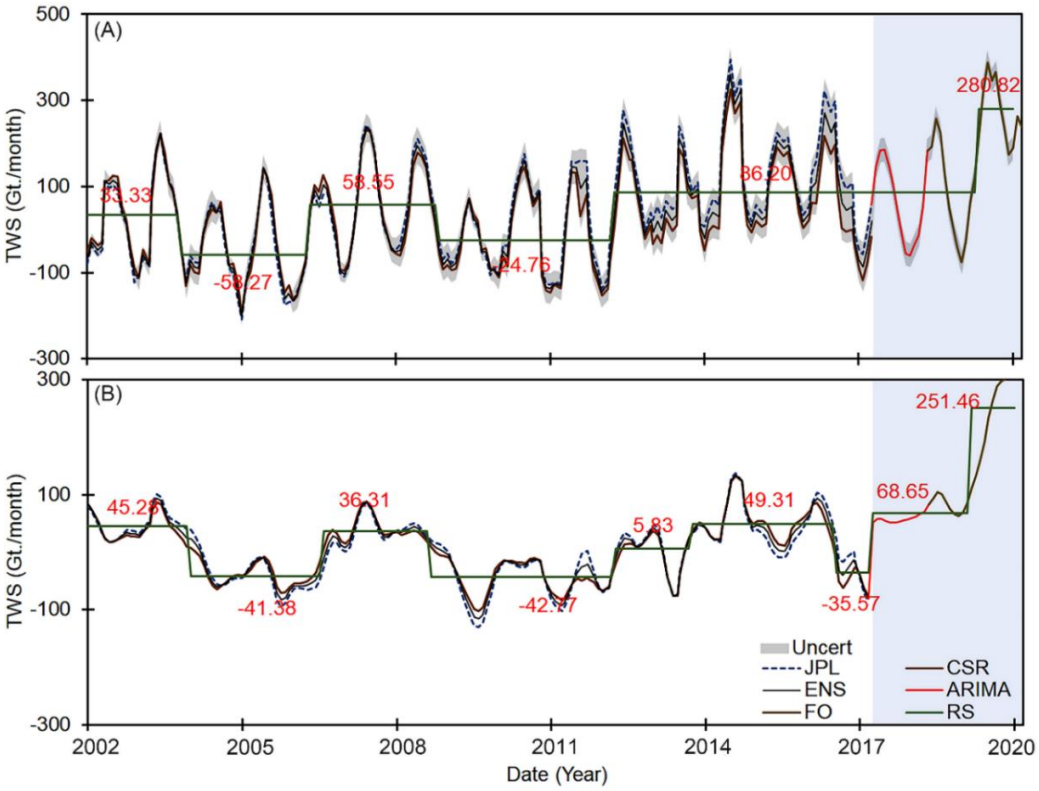

Figure 2. TWSA (A) and the cycle trend component (B) over the NRB using CSR, JPL, and Ensemble (ENS) mascons solutions between 2002-2017, the red lines represent the gap-filling between 2017-2018, the shaded area represents the GRACE-FO TWSA estimates between 2018-2020. The graph indicates the significant regime shift (RS) in the mean, the green line.

Figure 3 summarizes the change in the TWSA across the NRB during the wet (A), dry season (B), and the net change between the two for the period 2002 to 2020 (C). The plot shows that on average the NRB received storage between 50 Gt./yr. to approximately 310 Gt./yr. during the wet season. In contrast, dry season losses ranged between ~30 Gt./yr. to ~70 Gt./yr. As a result, the net TWSA change across the NRB showed a substantial increase from 2010 to 2020 of about 200 Gt./yr. on average. For additional details, the year-to-year rate of changes in the TWS, and the overall yearly changes compared to the mean annual average in TWS between 2002 to 2020 is presented in Figure S1A and S1B in the supplementary info.

Preprints (www.preprints.org) | NOT PEER-REVIEWED | Posted: 18 January 2021 doi:10.20944/preprints202101.0357.v1

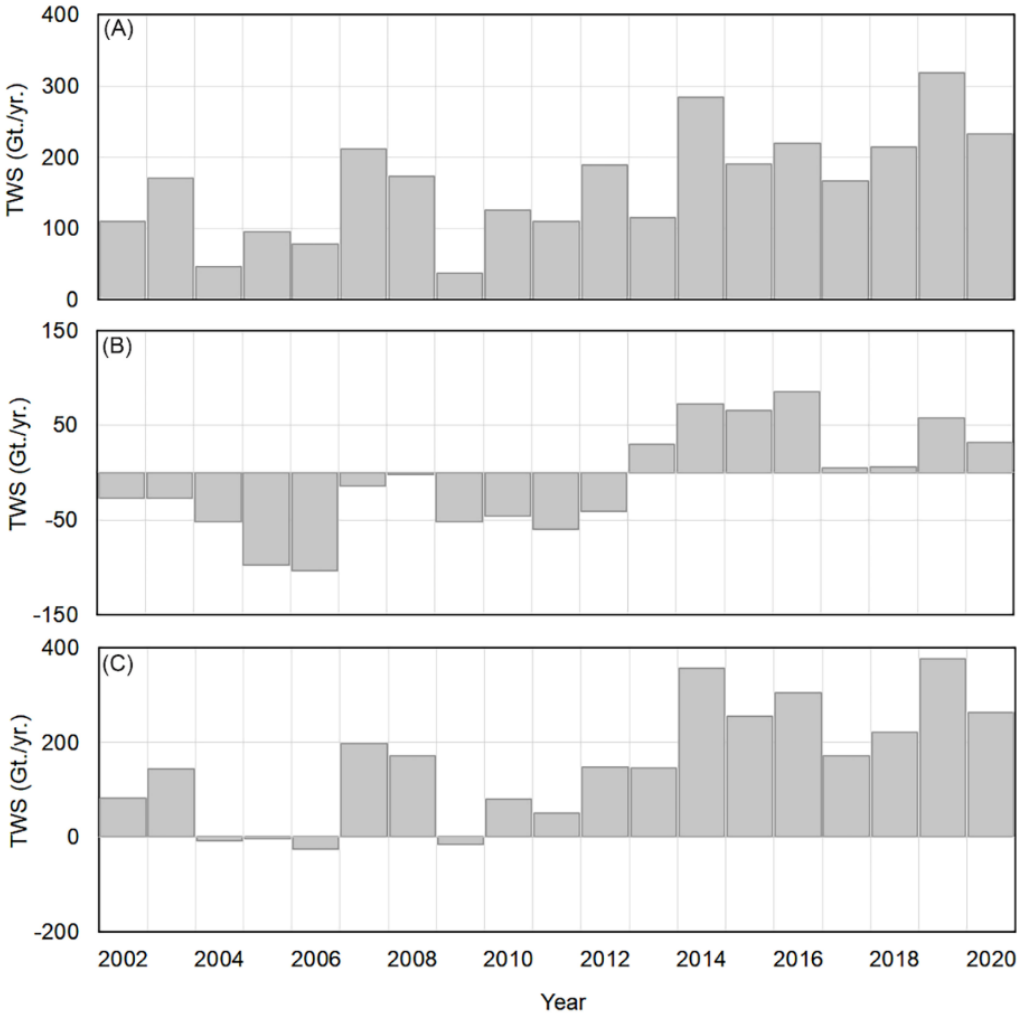

Figure 3. The total changes in TWS over NRB from 2002-2020 during the wet (A) and dry (B) seasons, plot (C) shows the total water storage during the two seasons.

Figure 4 shows similar TWSA dynamics during the wet and dry periods at two main source water areas (i.e., Lake Victoria and BNB) and two water sinks (the Sudd basin and the Main Nile in the northern portion). Figure 4 shows important contrasts between the Lake Victoria Basin and the BNB in terms of surface runoff and TWSA. Recall that the BNB contributes 57% of the surface runoff of the Nile Basin while the White Nile contributes approximately 30%, the TWSA suggests another pattern. For instance, during the wet season (Figure 4A), the Lake Victoria Basin stores, on average, twice as much as the BNB. Additionally, beginning as early as 2006, the Lake Victoria net annual storage increased significantly. During the dry season, TWSA at the Lake Victoria area indicates a general increasing pattern, except for the years 2005 and 2006. In the BNB, however, during the dry season the TWS improved continuously since 2002, it did not become positive until 2014. Figure 4C, suggests the net surplus in the TWSA; generally, the net pattern confirms the significant increase in the TWSA storage over the Lake Victoria water tower area compared to the BNB. Noteworthy, the years of 2005, 2006, and 2009 display the lowest TWSA records over the Lake Victoria region, the years between 2002 to 2005 present the lowest recorded TWSA over the BNB water tower region. The net storage between 2002 to 2020 was summarized across the three main sub-basins; BNB, WNB, and Atbara (see Figure S2).

Preprints (www.preprints.org) | NOT PEER-REVIEWED | Posted: 18 January 2021 doi:10.20944/preprints202101.0357.v1

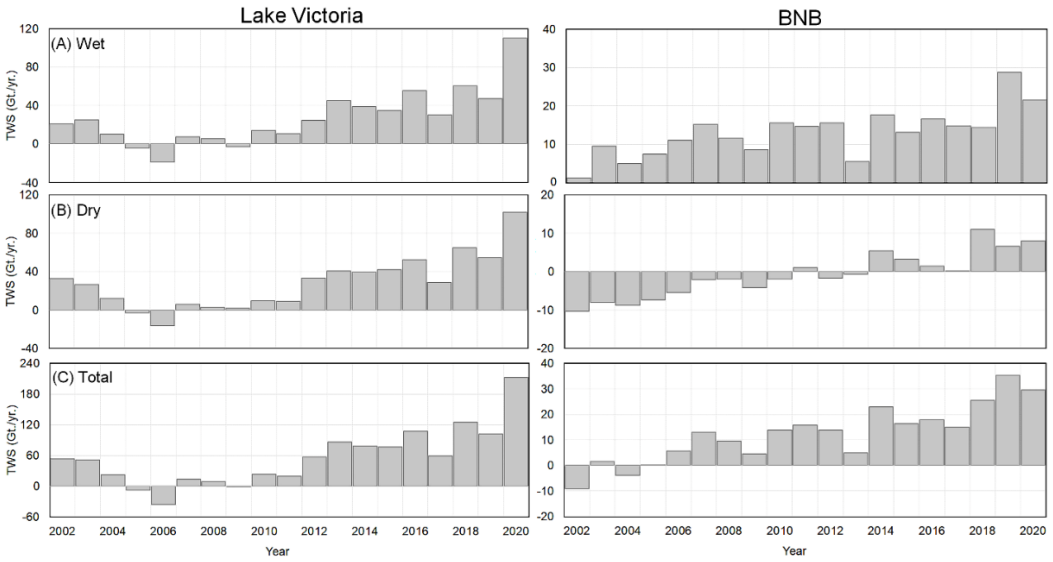

Figure 4. TWSA dynamics during the wet and dry seasons between 2002 to 2020 across the two main water towers in the NRB, Lake Victoria, and BNB water towers.

In the two water sink regions (Figure 5), the temporal patterns observed in the water source regions are flipped. That is, in both sink areas, net positive water storage occurred during the early part of the series followed by water deficits. For instance, during the wet season, Figure 5A, the Sudd basin receives an average TWS of ~8 Gt./yr. Two negative records of TWSA during the years of 2014 and 2016. In contrast, the Main Nile region shows a significant decline in the TWSA during the wet period, ranging from ~ 4 Gt./yr. in 2002 to –3 Gt./yr.in 2020. Both the Sudd basin and Main Nile regions display significant water volume losses during the dry period, Figure 5B. The Sudd basin displays an average of ~ –6 Gt./yr. during the wet period. For the Main Nile region, except for the period from 2002 to 2004, the TWSA displays significant negative records of ~ –3 Gt./yr. of water loss. The net change in TWSA over the regions, (Figure 5C), indicates that the Sudd basin exhibits a net record of positive storage between 2003 and 2008, and between 2014 to 2015. The Main Nile region, however, shows declining storage from ~4 to ~0.5 Gt./yr. between 2004 to 2005. The net TWSA change in the Main Nile region presents a continuous decline in TWSA between 2009 to 2020.

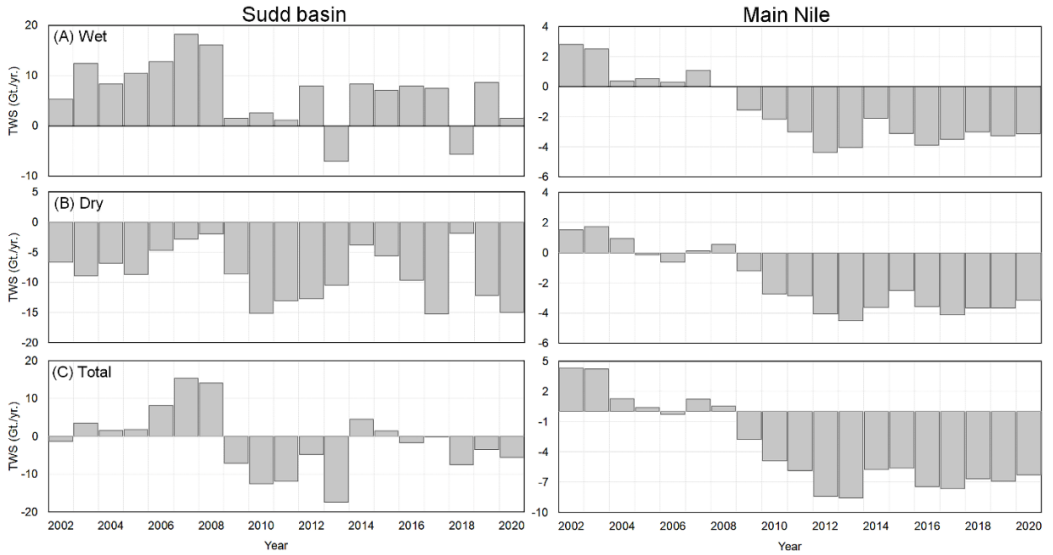

Figure 5. TWSA dynamics during the wet and dry seasons between 2002 to 2020 across the two main water sinks in the NRB, Sudd basin and Main Nile, and BNB.

Preprints (www.preprints.org) | NOT PEER-REVIEWED | Posted: 18 January 2021 doi:10.20944/preprints202101.0357.v1

Spatially, the distribution of TWSA across the NRB for the period between 2002 and 2017 based on ensemble SH06, CSR-M06, and JPL-M06 mason solutions appear in Figure 6. The patterns are consistent with the temporal trends reported in Figure 5. During the study period, the Equatorial Lake region had a positive increase of about 6+ cm/yr. while the sink region (Sudd basin, Sobat, and Bahr El-Jebel areas) experienced declines of between –2 cm/yr. and –4 cm/yr. The eastern portions of the WNB, BNB, and at confluence region of the White Nile and the Blue Nile rivers also had positive TWSA of between 2 cm/yr. to 4 cm/yr. Finally, the desert area in the northern portion of the basin declined by about –1.99 cm/yr. The standard deviation, Figure 6B, during the studied periods indicates a strong deviation from the mean, between 10 cm/yr. to 6 cm/yr., at the southern Equatorial Lake region, the WNB. The standard deviation degrades gradually to around 1 cm/yr. further to the northern portion of the basin.

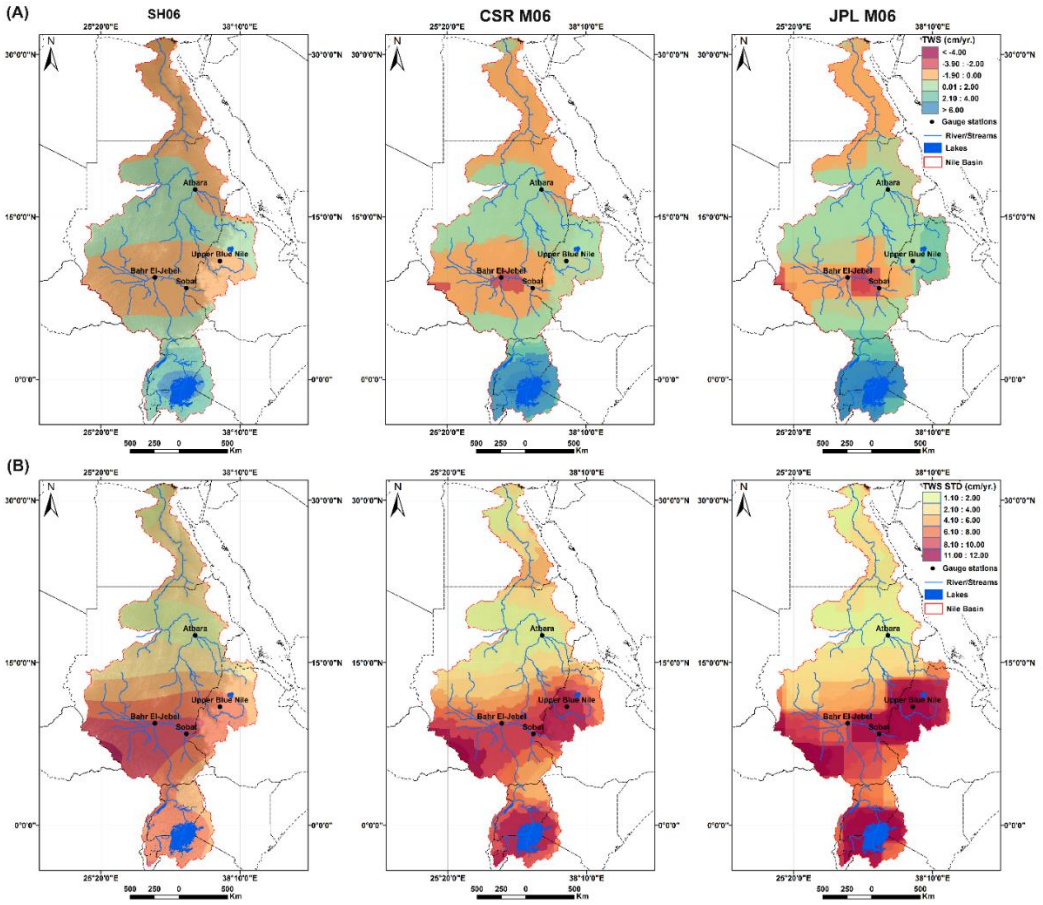

Figure 6. Mean annual average GRACE TWS (A) between 2002-2017 using ensembled SH06, CSR-M06, and JPL-M06 mascon solutions, plot (B) shows the standard deviation of each solution during the studied period.

Similarly, the mean annual average TWSA period between 2018 to 2020 is represented using GRACE-FO TWS estimates using an ensembled SH06, CSR-M, and JPL-M mascon solutions (Figure 7). Figure 7A shows the TWS distribution over the NRB between 2018 to 2020. Over the southern portion of the basin, the Equatorial Lake region exhibits a positive increase in TWS of 10+ cm/yr. Northwards over the Sudd basin, Sobat, and Bahr El-Jebel areas, the TWS fluctuates between +2 cm/yr. to -2 cm/yr. The western portion of the WNB, BNB area, and at the junction between the White Nile and the Blue Nile rivers display positive TWS that scale between 4 to 6 cm/yr. The desert area in the northern portion of the basin exhibits a significant decline in the TWS trajectories between –1.99 cm/yr. to –10 cm/yr. The standard deviation, Figure 7B, during the studied periods indicates a strong deviation from the mean, between 10 cm/yr. to 6 cm/yr., at the southern Equatorial

Preprints (www.preprints.org) | NOT PEER-REVIEWED | Posted: 18 January 2021 doi:10.20944/preprints202101.0357.v1

Lake region, the White Nile basin. The standard deviation degrades gradually to around 1 cm/yr. further toward the desert portion of the basin.

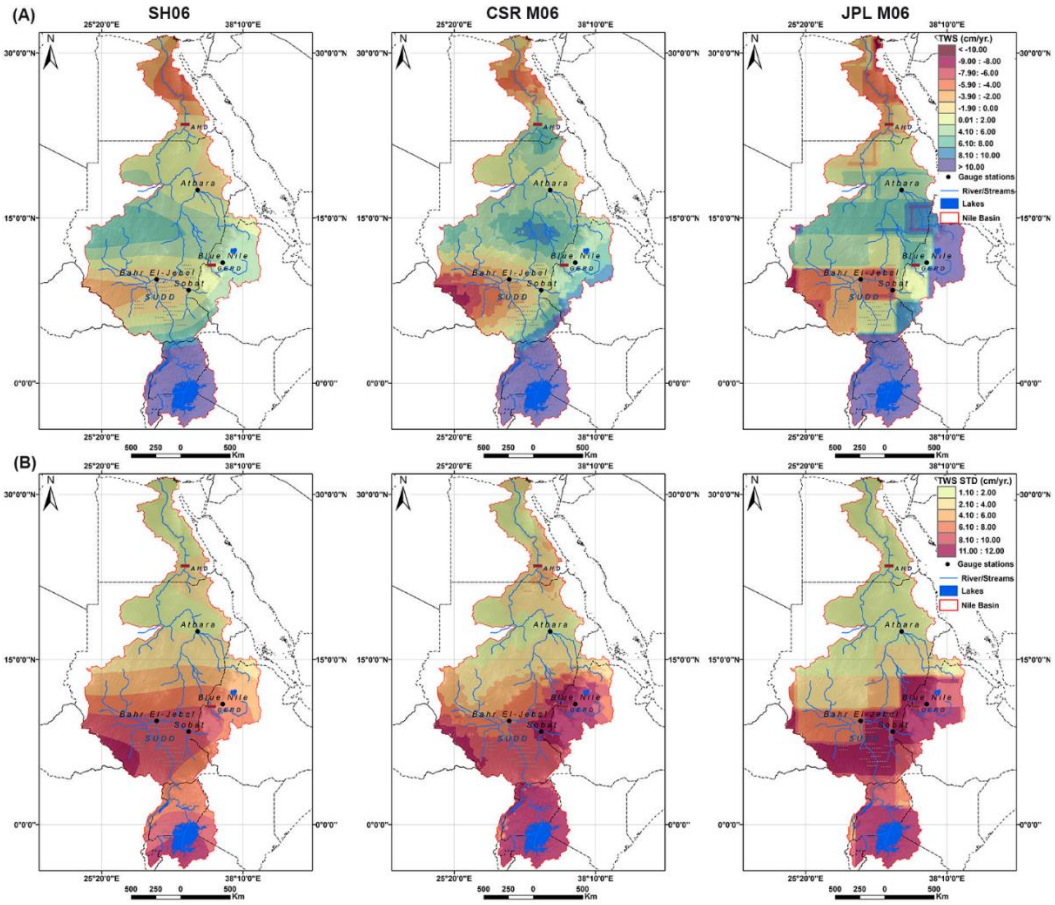

Figure 7. Mean annual average GRACE-FO TWS (A) between 2018- 2020 using ensembled SH06, CSR-M06, and JPL-M06 mascon solutions, plot (B) shows the standard deviation of each solution during the studied period.

The CRU precipitation records were evaluated against other independent precipitation estimates from the GPCC gauge corrected data using standardized coevolution approaches, see Figure S3A. The simulated/reconstructed TWSA was evaluated using standardized evaluation criteria including, coevolution between simulated TWSA and GRACE-based estimates (Figure 8A), cumulative distribution function (CDF) (Figure 8B), Pearson correlation coefficient (R-Square) (Figure 8C). Additionally, the historical simulated TWSA records were compared to CLSM-based TWSA estimates from 1948 to 2010 (Figure S3B). Other evaluation criteria utilized include the goodness-of-fit coefficients, Nash Sutcliffe efficiency (NSE), Root Mean Square Error (RMSE), (see Table S5), and residuals plots (see supplementary info Figure S4 for additional details). The uncertainty bounds in the simulated TWSA were calculated according to the approach described earlier (see previous section 3.7). Overall, during the training period, the results show strong agreement between simulated TWSA and GRACE-based estimates with R-Square of 0.86 (p-value <0.0001), and closely related CDF curves. The results revealed a similarly strong agreement between the two estimates, p-value <0.0001. Besides, an indirect comparison of the historical TWSA records was established through the inter-comparison of the TWSD indicator to other independent drought indicators as well as precipitation anomalies, see section 4.5.2.

Preprints (www.preprints.org) | NOT PEER-REVIEWED | Posted: 18 January 2021 doi:10.20944/preprints202101.0357.v1

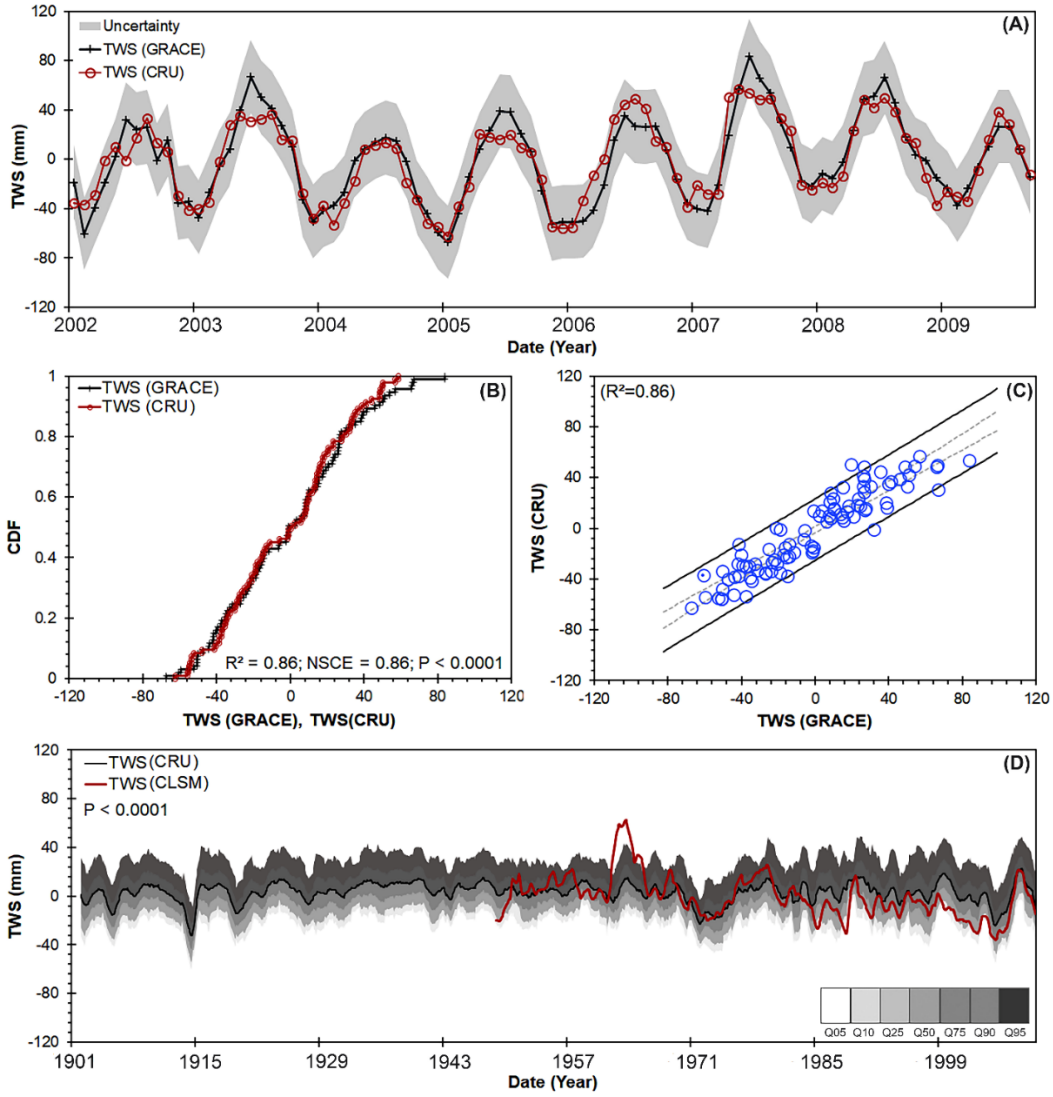

Figure 8. The model performance of the simulated TWS compared to ensemble GARCE-based TWS estimates (A).

4.3. Past TWS changes in the NRB (1901-2002)

The monthly reconstructed TWSA was developed for the period before GRACE-era between 1901 to 2002 (see Figure S3B in the supplementary info). Figure 9 summarizes the general temporal pattern of the reconstructed TWSA using mean annual TWSA estimates during the wet (Figure 9A) and the dry (Figure 9B). The results show insubstantial yearly variation in the TWSA across the NRB. During the wet period, Figure 9A, three eras of changes in the TWSA annual mean (regime shift), between 1901 to 1951 with ~98 Gt./yr. of TWS. Then, between 1952 to 1979, the mean annual TWSA peaked at ~133 Gt./yr. During the period from 1980 to 2002, the mean annual TWSA slightly decrease to 114 Gt./yr. The dry period, Figure 8B, also showed slight temporal changes in the TWSA annual average with two identified periods of ~–56 Gt./yr. of storage reduction between 1901 to 1960, and ~–40 Gt./yr. from 1961 to 2002.

Preprints (www.preprints.org) | NOT PEER-REVIEWED | Posted: 18 January 2021 doi:10.20944/preprints202101.0357.v1

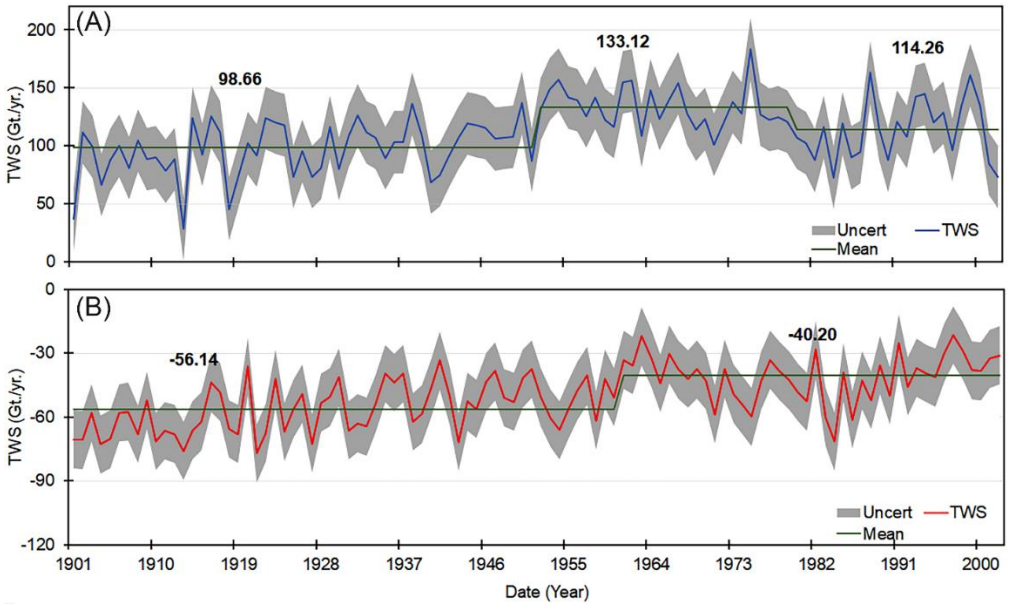

Figure 9. Reconstructed TWS in the NRB between 1901 to 2002 during the wet (A) and dry period (B).

4.4. Future TWS scenarios in NRB (2021 to 2050)

The TWSA in the NRB region was projected for the period 2021 and 2050, Figure S3C shows the monthly projected TWSA record. The future precipitation and temperature records were used to estimate the TWSA following the methodology reported in section 3.5. Figure 10 summarizes the overall temporal variability in the TWSA estimates using mean annual average records during the wet (Figure 10A) and the dry (Figure 10B) seasons. Three main regions of TWSA regime shift were recorded, between 2021 to 2025, 2026 to 2035, and from 2036 to 2050. The projected TWSA records suggest slight positive changes in the TWSA mean during the dry period across the basin.

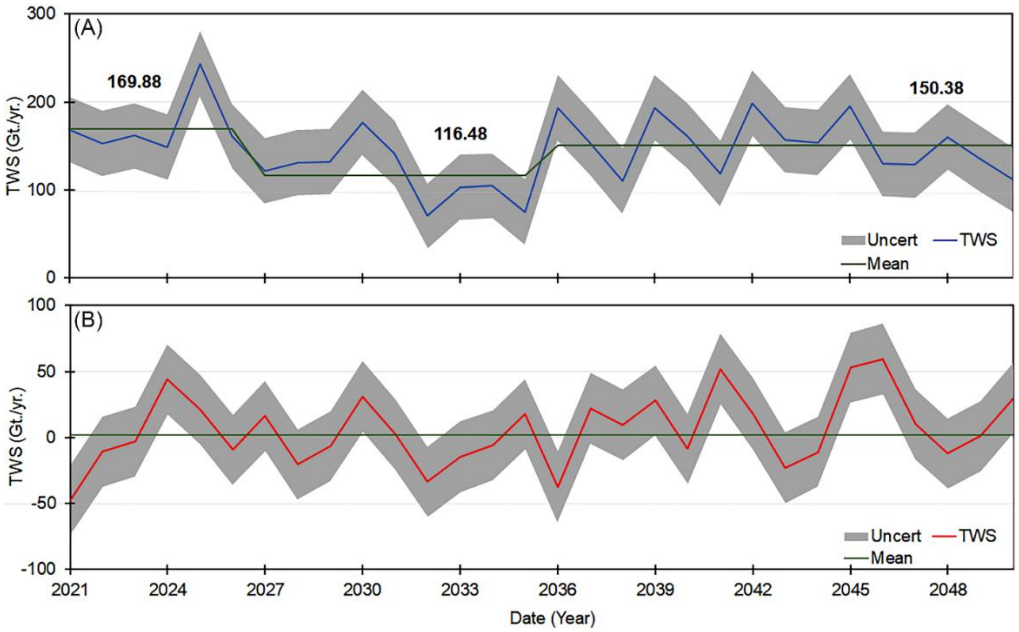

Figure 10. The projected changes in mean TWS between 2021 to 2050 in the NRB during wet (A) and dry (B) seasons.

4.5. Drought and Flooding in the NRB

Preprints (www.preprints.org) | NOT PEER-REVIEWED | Posted: 18 January 2021 doi:10.20944/preprints202101.0357.v1

4.5.1. GRACE- based TWSD between 2002 to 2020

Figure 11 shows the yearly TWSD across the NRB between 2002 to 2020 using ensemble SH06 data. Table S2 shows the standard thresholds for the TWSD levels. As may be expected for a large and heterogenous basin. Spatially, the TWSD varies from extremely wet to extremely dry conditions for different portions of the basin. For example, the Equatorial Lake region in the south portion of the basin was characterized by abnormally dry (D0) in 2002 to exceptional drought conditions (D4) between 2005 and 2006. During the next two years, however, the region recovered to near normal status. On the other hand, the main stem of the Nile experienced generally moderate to favorable drought conditions between 2002 and 2007 but adverse drought conditions between 2014 and 2018. For most of the basin, the years 2007, 2008, 2014, and 2018 were wet to abnormally wet while 2004, 2006, 2017, and 2019 were abnormally dry.

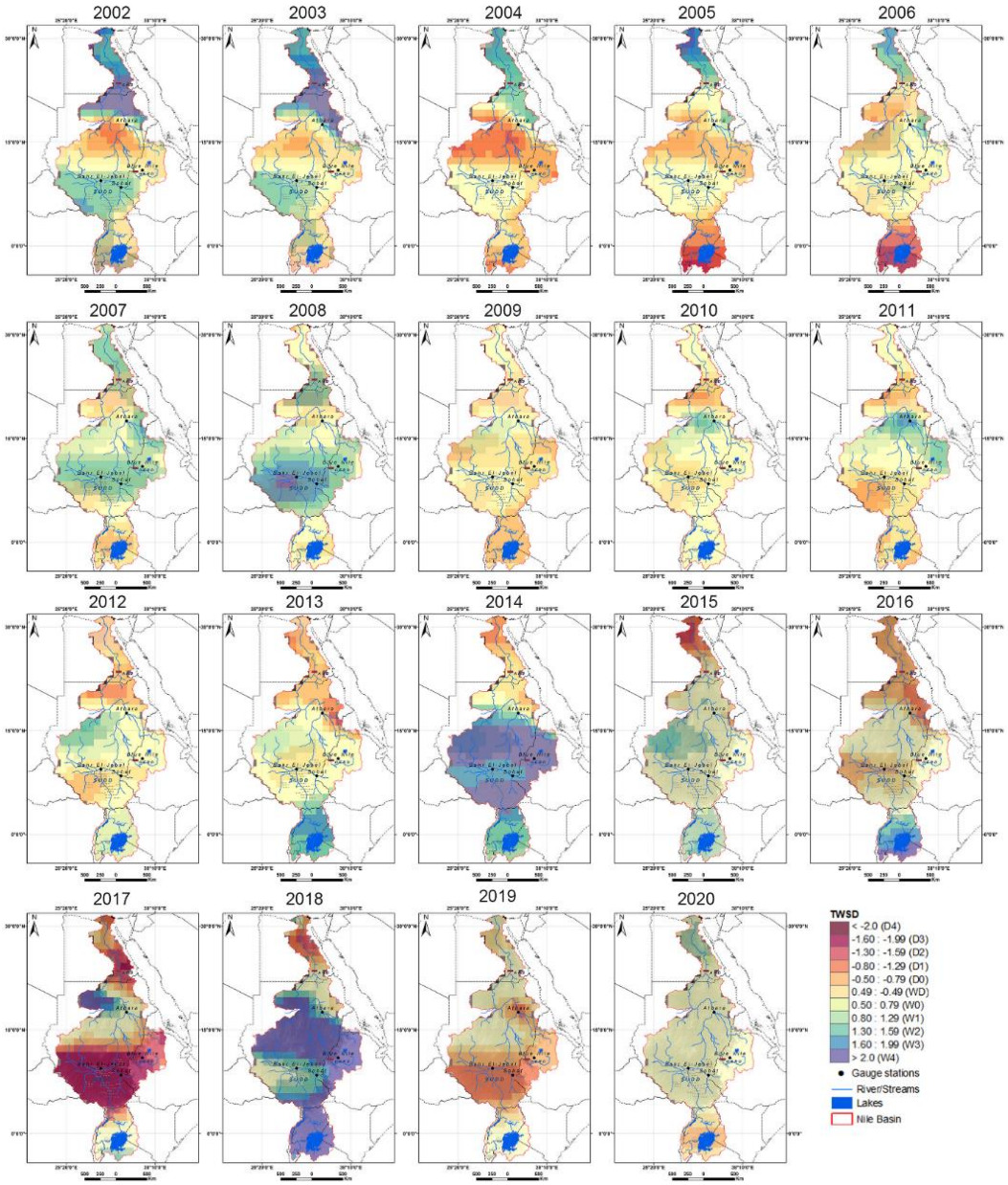

Figure 11. The spatial pattern of the TWSD over the NRB between 2002 to 2020.

Other regions across the basin showed remarkable dryness and wetness records between 2002 to 2020. The western portion of the White Nile at Bahr El Jabel area, for

Preprints (www.preprints.org) | NOT PEER-REVIEWED | Posted: 18 January 2021 doi:10.20944/preprints202101.0357.v1

instance, exhibits moderate to very wet conditions during the years of 2002, 2003, 2007, and the year 2008. The year 2014 and 2018 show extreme wet conditions. The Bahr El Jabel region demonstrates normal conditions for the period between 2004 to 2006, and the years of 2009, 2010, 2013, and 2020. In the years 2017 and 2019, the Bahr El Jabel region records extreme dry conditions to a moderate dry condition respectively. The northern portion of the White Nile Basin at the junction between the White Nile and the Blue Nile rivers fluctuates from moderate drought in 2002 to severe drought conditions in 2004. Slightly dry condition record in 2005, then a progressive recovery started from 2006 to the year 2008 with very wet condition status. The years 2014 and 2018 show exceptionally wet conditions across the region. The BNB region ranks from the normal condition in 2002 to moderately dry conditions in 2004 and 2005. The severity levels show recovered conditions in the years 2007 and 2008. Extreme dry conditions were recorded in 2017, then the 2018 scores toward the extremely wet conditions.

4.5.2. NRB drought and flooding records (1901 to 2050)

Historical, current, and future drought and flooding events were established using statistical-based TWSD between 1901 to 2050. The TWSD records were compared to other standardized drought indicators including SPI, SPEI, scSPDI, PDSI, GPCC_DI, and TWSD indicators, along with the precipitation anomaly in the basin. Figure 12 shows both droughts (-2) and flooding (+2) records from standardized drought indices. Noteworthy, the inter-comparison between each drought indicator and precipitation anomalies indicates strong temporal coevolution (p-value 0.0001). According to table S1, Figure 12 clearly illustrates different exceptionally dry periods, i.e., during the years of 1913, 1918, 1943, 1984, 1987, 1990, 1992, 2004, and 2009. Additionally, remarkable wet periods were noted during the years 1917, 1924, 1930 to 1940, 1964, 1989, 2000, 2007, 2014, and the year 2020. Between 2021 to 2050, the future TWSD record indicates fewer dry conditions relative to normal, and slightly wetter conditions.

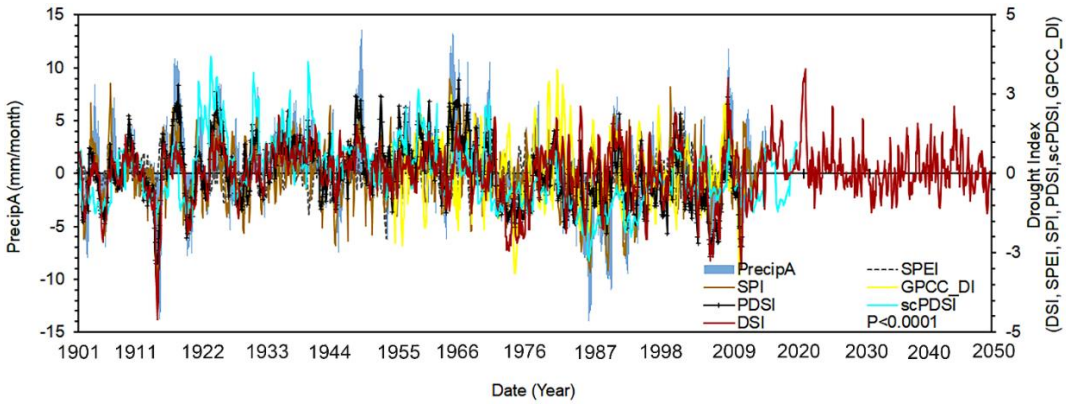

Figure 12. Standardized drought indicators in the NRB compared to precipitation anomalies between 1901 to 2020.

Analysis of the entire reconstructed (retrogressive/inclusive), present, and projected (exclusive) periods (1901 to 2050) shows that the NRB has more wet periods (86 years) compared to 64 years of dry record (Figure 13). While the dry years are fewer, they tend to be deeper. For example, both the droughts of 1912 and 1971-73 exceeded -2.0 on the DSI scale. Furthermore, the wet and dry years tend to occur as runs. The longest wet run-length occurred during the decade from 1931-1940. The longest dry run occurred between 200 and 2006. Finally, the projection suggests that future wet and dry periods in the Niger Basin will be mild compared to the historical period

Preprints (www.preprints.org) | NOT PEER-REVIEWED | Posted: 18 January 2021 doi:10.20944/preprints202101.0357.v1

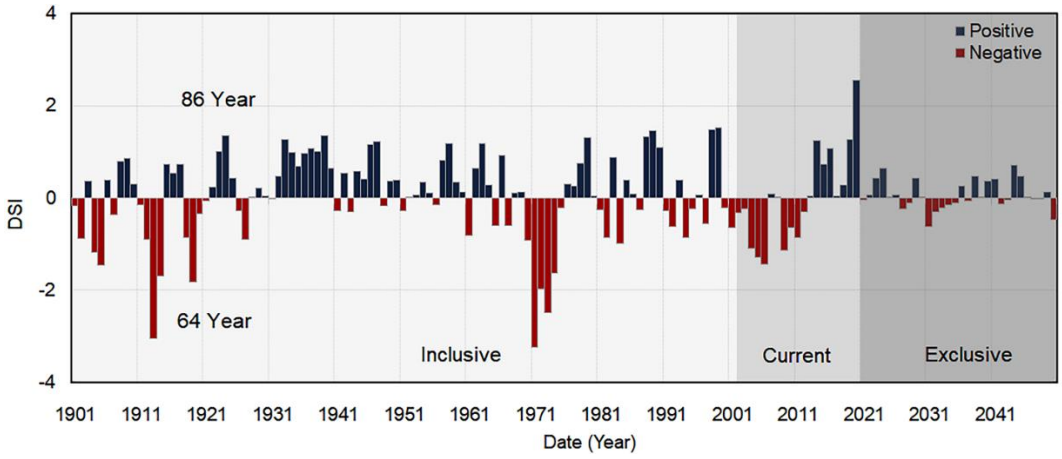

Figure 13. The dry and wet months in the NRB between 1901 to 2050.

Figure 14 summarizes the drought and flooding recurrence intervals and frequencies in the NRB between 1901 to 2050. The frequency analysis indicates that the NRB has short drought and flooding intervals of ~6 years recurrence intervals. The longer recurrence periods in the basin are less likely to occur. The analysis also shows that from 1901 to 2050, the recurrences of the drought events are less intense compared to the flooding record that significantly displays higher reoccurrence intervals with time.

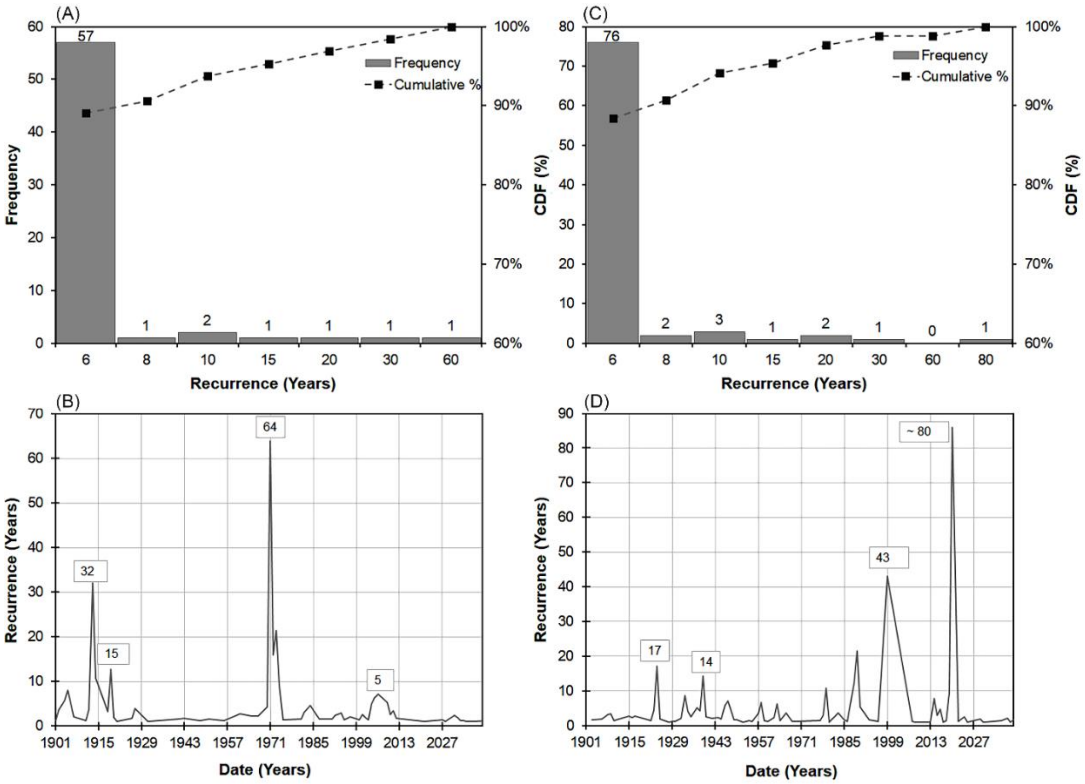

Figure 14. Drought frequency (A) and recurrence and flooding frequency (C) and recurrence (D) between 1901-2050.

5. Discussion

The GRACE and GRACE-FO TWSA records between 2002 to 2020 indicate that the NRB is experiencing a humid phase. A review of existing research showed that the maximum reported water storage from surface water flow in the NRB is ~100 BCM/yr. [74].

 doi:10.20944/preprints202101.0357.v1

Herein, however, our analysis shows that the total available water storage from all sources (surface, groundwater storage) is on the order of 200 BCM/yr., nearly double the previous estimate (see Figure S5). Several factors may account for the differences between the TWS amount reported here and previous estimates. First GRACE based TWS estimates that includes all water storage down to the deepest levels of the aquifer, including water locked away in fossil or hydrologically inactive aquifers. As such, there is an important caveat to these new storage figures; the total amount of available water cannot all be extracted and used due to technological and economic constraints. Therefore, the new figure likely overestimates the amount of useable storage within the basin. Despite such differences, GRACE derived TWS estimates have the advantage of being spatially distributed rather than lumped as in most previous estimates. It also most likely that the conventional water budget-based approach underestimates the total amount of water storage within the basin. Moreover, even with these new higher storage estimates, the basin would still be considered a water-stressed [47] based on current and projected population.

While other research studies on the NRB utilized lumped/basin-average TWSA estimates, i.e., [43]. This current study explicitly acknowledges the spatial variability of TWSA at different parts of the NRB region; Spatially, the TWS displays uneven storage patterns across the region. The Equatorial Lake region, the White Nile basin, and the BNB, for instance, show positive TWSA records with higher standard deviation values due to the strong seasonal amplitude fluctuations. The northern portion of the basin, on the other hand, displays a remarkable decline in the TWS values with low standard deviation values due to minimal seasonal amplitudes. Moreover, analysis of the TWS at mascon-level across two main water towers (Lake Victoria and BNB), and two other water sink regions (Sudd basin and Main Nile), specifies the TWSA dynamics during the GRACE and GRACE-FO era.

Our results highlight another aspect of the Nile Basin hydrology not generally appreciated. That is, while the BNB contributes 86 percent of the Nile runoff, the White Nile Basin holds twice the total water storage of the BNB. This is important because the NRB is sensitive to changes in the TWSA; an increase/decrease of +/- ~2 cm of TWS across the basin would increase/decrease the total available storage by (+/-) ~60 percent. Accurate information on the available water storage greatly facilitates water resources planning and management throughout the basin.

Before GRACE-era, the reconstructed TWSA record showed that between 1901 to 2002 the wet-months are more frequent compared to the dry-month in the region. The projected TWS indicated insignificant TWS changes during the dry seasons compared to normal, and slightly wetter conditions during the wet seasons. These projections are compared favorably with those reported by e.g., [42, 48] that showed a trend towards increased water resources in the NRB and considerable changes. For example, the increased TWS is likely driven by the projected increase in precipitation over the basin during the next five decades. While the temperature will also likely increase, the net precipitation increase exceeds the expected higher water losses via ET due to higher temp [18]. There are good grounds for presuming that such changes result from global warming, whose intensity has increased considerably in the last few decades. Historical drought and flooding records in the NRB showed that six feet (~2 meters) of waters in the river channel above/below normal during flood/drought season could bring life and prosperity to the land, and renew its fertility. Or, could bring severe drought, famine, and would reduce the agriculture yields to three-quarters [75]. Therefore, establishing an intrinsic water-sharing agreement among riparian nations to govern the water resources allocation in the region is needed more than ever. It is not an easy task for the 11 countries in the basin to agree to a water-sharing plan. But the key to ensuring cooperation among riparian states is good information sharing and technical cooperation to avoid chronic water shortages in the future.

 doi:10.20944/preprints202101.0357.v1

6. Summary and conclusion

TWS is critical to understanding the water availability and changes in the NRB. This research analyzed the current TWSA using GRACE and GRACE-FO records from 2002 to 2020. Then, data-driven TWSA records for the pre-GRACE-era between 1901 to 2002, and projected forward the TWSA record between 2021 to 2050. The results showed the following key findings.

- GRACE TWSA records between 2002 to 2020 indicate that the NRB is experiencing a generally humid phase. In the year 2020, for example, the TWS was ~8-times higher than in the year 2002.
- The basin-wide TWSA from GRACE shows significantly higher storage amounts compared to TWSA estimates using LSM outputs (i.e., 200 BCM vs. 100 BCM). The discrepancy in the TWSA estimates is likely due to the fact that the GRACE satellite to detect all forms of available storage, including the deep groundwater component, as well as the anthropogenic influence on different water stocks.
- While the BNB contributes 86 percent of the surface runoff measured in the Nile River, the Lake Victoria source region holds at least twice as much water storage during the wet season.
- The future projections of TWSA indicate insignificant changes during the wet and dry seasons of the projected TWSA compared to the overall mean average. The reason for this is likely related to the projected increase in the precipitation amount in the region.

The complex hydrology and social-environmental systems in the Nile Basin historically have required delicate negotiations and management. Future dynamics related to population growth, climate change, and the socio-economic and political decisions of the countries which cohabit the Nile Basin will require an ever-increasing amount of information regarding the shared resources of the Nile Basin of which water is by far the most important. This study demonstrates that GRACE data can provide unique new insights and perspectives relevant to the sustainable management of water resources in the Nile Basin.

Supplementary Materials: The following are available online at www.mdpi.com/xxx/s1, Figure S1: NRB year-to-year TWSA changes (A) between 2002 to 2020, and the yearly changes (compared to the overall average) in the TWSA (B), Figure S2: GRACE-TWSA-based net storage between 2002 to 2020 across BNB (A), WNB (B) and Atbara sub-basins, Figure S3: Coevolution between monthly GPCC and CRU precipitation data (A), and GAMLSS-based TWSA and CLMS TWSA (B). Plot C shows the monthly projected TWSA, Figure S4: Simulated ARIMA TWS (A), the dark below of the plot is the one-year gap, and the residual plot of the model (B), Figure S5: NRB storage figures from TWS (A), GWS (B), SMS (C), and runoff (D) between 1948 to 2014 of CLSM-F2.5 LSM. The storage-based figures are relatively high relative to the runoff in the basin, Table S1: Source information for datasets and drought indicators utilized in this research, Table S2: Standard thresholds used to identify the drought severity levels, Table S2: Standard thresholds used to identify the drought severity levels, Table S3: Summary of the regime-shift analysis of the NRB mean TWS between 2002 to 2020, Table S4: Summary of the regime-shift analysis of the NRB in the TWS cyclic component between 2002 to 2020. Table S5: GAMLESS (A) and ARIMA (B) models' goodness-of-fit criteria.

Author Contributions: Conceptualization, E. Hasan and A. Tarhule; methodology, E. Hasan, and P. E. Kirstetter; Validation, E. Hasan, and P. E. Kirstetter; formal analysis, E. Hasan, P. E. Kirstetter, and A. Tarhule; writing—review and editing, E. Hasan and A. Tarhule; Supervision and Funding acquisition, A. Tarhule.

Funding: This research was funded by The Provost Office at Binghamton University.

Data Availability Statement: This study was performed based on public-access data. Data utilized in this research can be requested by contacting the first author at a reasonable request.

Acknowledgments: The authors thank the Provost's office at the State University of New York (SUNY) at Binghamton for providing research funds for this study. Thanks also go to the provost office at Illinois State University, Normal, IL, the USA for supporting this research.

We also wish to thank the three GRACE data centers; Center for Space Research (CSR) at the University of Texas, Austin, the Jet Propulsion Laboratory (JPL, NASA California, USA), and the Deutsches GeoForschungsZentrum (GFZ, Potsdam, Germany), the GRACE Tellus and the Physical Oceanography Distributed Active Archive Center (PO.DAAC) for the data access. We also wish to NASA Goddard Earth Science Data and Information Service Centers, the CRU, GPCC, for various datasets used in this work.

Conflicts of Interest: The authors declare no conflict of interest.

References

1. Shahin, M., *Hydrology of the Nile Basin*. 1985, New York: Elsevier Science Publishing Company Inc.
2. Sutcliffe, J.V. and Y.P. Parks, *The Hydrology of the Nile*. 1999, Colombo. Sri Lanka: The International Water Management Institute. IAHS Special Publication no. 5.
3. Collins, R., *The Nile*. 2002: Yale University Press/ New Haven and London.
4. Said, R., *The geological evolution of the River Nile*. 1981: Springerverleg.
5. Swain, A., *Challenges for water sharing in the Nile basin: changing geo-politics and changing climate.* Hydrological Sciences Journal, 2011. **56**(4): p. 687-702.
6. Karyabwite, D.R., *Water Sharing in the Nile River Valley*, in *United Nations Environment Programme (UNEP)* 2000 UNEP/DEWA/GRID, Geneva.
7. Oestigaard, T., *Nile Issues, Small Streams from the Nile Basin Research Programme*. 2010, Kampala-Uganda: Fountain Publishers.
8. Arsano, Y., *Ethiopia and the Nile*. Dilemmas of National and Regional Hydropolitics. 2007, ETH Zurich: Center for Security Studies (CSS). 324.
9. NBI, *Nile Basin Water Resources Atlas*, A.H. Seid, M. Mbuliro, and M. Alarabawy, Editors. 2017.
10. Haub, C. and T. Kaneda, *2013 World Population Data Sheet – Population Reference Bureau*. 2013.
11. Abu-Zeid, M., *The river Nile: main water transfer projects in Egypt and impacts on Egyptian agriculture*, in *Long-distance water transfer*, B.A.K.e. al., Editor. 1983, Tycooly International Publishing Ltd: Dublin. p. 6–34.
12. Basheer, M., et al., *Quantifying and evaluating the impacts of cooperation in transboundary river basins on the Water-Energy-Food nexus: The Blue Nile Basin.* Sci Total Environ, 2018. **630**: p. 1309-1323.
13. Oestigaard, T., *Water Scarcity and Food Security along the Nile Politics, population increase and climate change*. 2012, Uppsala: Nordiska Afrikainstitutet.
14. Ayele, H., et al., *Impact of Climate Change on Runoff in the Gilgel Abbay Watershed, the Upper Blue Nile Basin, Ethiopia.* Water, 2016. **8**(9).
15. Conway, D., *Water resources: Future Nile river flows.* Nature Climate Change, 2017. **7**(5): p. 319-320.
16. Dessie, M., et al., *Analyzing runoff processes through conceptual hydrological modeling in the Upper Blue Nile Basin, Ethiopia.* Hydrology and Earth System Sciences, 2014. **18**(12): p. 5149-5167.
17. Gleick, P.H., *The vulnerability of runoff in the Nile basin to climatic changes.* The Environmental Professional, 1991. **13**: p. 66-73.
18. Hasan, E., et al., *Runoff sensitivity to climate change in the Nile River Basin.* Journal of Hydrology, 2018. **561**: p. 312-321.
19. Hurni, H., K. Tato, and G. Zeleke, *The Implications of Changes in Population, Land Use, and Land Management for Surface Runoff in the Upper Nile Basin Area of Ethiopia.* Mountain Research and Development 2005. **25** (2): p. 147–154.
20. Kebede, S., et al., *Water balance of Lake Tana and its sensitivity to fluctuations in rainfall, Blue Nile basin, Ethiopia.* Journal of Hydrology, 2006. **316**(1-4): p. 233-247.
21. Swenson, S. and J. Wahr, *Monitoring the water balance of Lake Victoria, East Africa, from space.* Journal of Hydrology, 2009. **370**(1-4): p. 163-176.

22. Awange, J.L., et al., *Water storage changes and climate variability within the Nile Basin between 2002 and 2011.* Advances in Water Resources, 2014. **73**: p. 1-15.
23. Khaki, M. and J. Awange, *Improved remotely sensed satellite products for studying Lake Victoria's water storage changes.* Sci Total Environ, 2019. **652**: p. 915-926.
24. Bonsor, H.C., et al., *Interpretation of GRACE data of the Nile Basin using a groundwater recharge model.* Hydrology and Earth System Sciences Discussions, 2010. **7**(4): p. 4501-4533.
25. Hasan, E., et al., *Assessing Lake Level Variability and Water Availability in Lake Tana, Ethiopia using a Groundwater Flow Model and GRACE Satellite Data*, in *AGU Fall Meeting*. 2017: New Orleans 11-15 Dec. 2017.
26. Shamsudduha, M., R.G. Taylor, and L. Longuevergne, *Monitoring groundwater storage changes in the highly seasonal humid tropics: Validation of GRACE measurements in the Bengal Basin.* Water Resources Research, 2012. **48**(2): p. n/a-n/a.
27. Conway, D., *From headwater tributaries to international river: Observing and adapting to climate variability and change in the Nile basin.* Global Environmental Change, 2005. **15**(2): p. 99-114.
28. Conway, D. and M. Hulme, *The Impacts of Climate Variability and Future Climate Change in the Nile Basin on Water Resources in Egypt.* International Journal of Water Resources Development, 1996. **12**(3): p. 277-296.
29. Hasan, E. and A. Tarhule, *GRACE: Gravity Recovery and Climate Experiment long-term trend investigation over the Nile River Basin: Spatial variability drivers.* Journal of Hydrology, 2020. **586**.
30. Hasan, E., et al., *+50 Years of Terrestrial Hydroclimatic Variability in Africa's Transboundary Waters.* Sci Rep, 2019. **9**(1): p. 12327.
31. Hassan, A. and S. Jin, *Water storage changes and balances in Africa observed by GRACE and hydrologic models.* Geodesy and Geodynamics, 2016. **7**(1): p. 39-49.
32. Hasan, E., et al., *The Challenges and Opportunities of Hydrologic Remote Sensing in Data-Poor Regions: Case Study of Nile River Basin.* AGU Fall Meeting Abstracts, 2015. **51**: p. H51T-07.
33. Anyah, R.O., et al., *Understanding linkages between global climate indices and terrestrial water storage changes over Africa using GRACE products.* Sci Total Environ, 2018. **635**: p. 1405-1416.
34. Khaki, M., et al., *Understanding the association between climate variability and the Nile's water level fluctuations and water storage changes during 1992-2016.* Sci Total Environ, 2018. **645**: p. 1509-1521.
35. Swenson, S., et al., *Estimating profile soil moisture and groundwater variations using GRACE and Oklahoma Mesonet soil moisture data.* Water Resources Research, 2008. **44**(1): p. 1-12.
36. Swenson, S. and J. Wahr, *Estimating Large-Scale Precipitation Minus Evapotranspiration from GRACE Satellite Gravity Measurements.* Journal of Hydrometeorology, 2006. **7**: p. 252-270.
37. Tapley, B.D., et al., *GRACE Measurements of Mass Variability in the Earth System.* Science, 2004. **305**(5683): p. 503.
38. Tapley, B.D., et al., *Contributions of GRACE to understanding climate change.* Nature Climate Change, 2019. **9**(5): p. 358-369.
39. Scanlon, B.R., et al., *Tracking Seasonal Fluctuations in Land Water Storage Using Global Models and GRACE Satellites.* Geophysical Research Letters, 2019.
40. Scanlon, B.R., et al., *Global models underestimate large decadal declining and rising water storage trends relative to GRACE satellite data.* Proc Natl Acad Sci U S A, 2018. **115**(6): p. E1080-E1089.
41. Elshamy, M.E., I.A. Seierstad, and A. Sorteberg, *Impacts of climate change on Blue Nile flows using bias-corrected GCM scenarios.* Hydrology and Earth System Sciences, 2009. **13**(5): p. 551-565.
42. Siam, M.S. and E.A.B. Eltahir, *Climate change enhances interannual variability of the Nile river flow.* Nature Climate Change, 2017. **7**(5): p. 350-354.
43. Shamsudduha, M., et al., *Recent changes in terrestrial water storage in the Upper Nile Basin: an evaluation of commonly used gridded GRACE products.* Hydrology and Earth System Sciences, 2017. **21**(9): p. 4533-4549.
44. Dile, Y.T., R. Berndtsson, and S.G. Setegn, *Hydrological response to climate change for Gilgel Abay River, in the Lake Tana Basin - Upper Blue Nile Basin of Ethiopia.* PLoS One, 2013. **8**(10): p. e79296.

45. Senay, G.B., et al., *Understanding the hydrologic sources and sinks in the Nile Basin using multisource climate and remote sensing data sets.* Water Resources Research, 2014. **50**(11): p. 8625-8650.
46. Sutcliffe, J. and E. Brown, *Water losses from the Sudd.* Hydrological Sciences Journal, 2018. **63**(4): p. 527-541.
47. Hasan, E., et al., *Assessment of Physical Water Scarcity in Africa Using GRACE and TRMM Satellite Data.* Remote Sensing, 2019. **11**(8).
48. Coffel, E.D., et al., *Future Hot and Dry Years Worsen Nile Basin Water Scarcity Despite Projected Precipitation Increases.* Earth's Future, 2019. **7**(8): p. 967-977.
49. Moges, S.A. and M. Gebremichael, *Climate Change Impacts and Development-Based Adaptation Pathway to the Nile River Basin.* . River Basin. 2014: Springer International Publishing Switzerland.
50. Abu-Zeid, M. and I.A. Shiklomanov, *Water Resources as A Challenge of the Twenty-First Century*. 2004: World Meteorological Organization.
51. Woodward, J., D. Welsby, and M. Macklin, *The Holocene fluvial sedimentary record and alluvial geoarchaeology in the Nile Valley of northern Sudan*, in *River Basin Sediment Systems - Archives of Environmental Change*. 2001.
52. Camberlin, P., *Nile Basin Climates*, in *The Nile : Origin, Environments, Limnology and Human Use*, H.J. Dumont, Editor. 2009, Springer, Monographiae Biologicae. p. 307-333.
53. NBI, *State of River Nile Basin 2012. Nile Basin Initiative (NBI), Entebbe.* 2012.
54. Landerer, F.W. and S.C. Swenson, *Accuracy of scaled GRACE terrestrial water storage estimates.* Water Resources Research, 2012. **48**(4): p. 1-11.
55. Save, H., *CSR GRACE RL06 Mascon Solutions*, H. Save, Editor. 2019, Texas Data Repository Dataverse.
56. Save, H., S. Bettadpur, and B.D. Tapley, *High-resolution CSR GRACE RL05 mascons.* Journal of Geophysical Research: Solid Earth, 2016. **121**(10): p. 7547-7569.
57. Watkins, M.M., et al., *Improved methods for observing Earth's time variable mass distribution with GRACE using spherical cap mascons.* Journal of Geophysical Research: Solid Earth, 2015. **120**(4): p. 2648-2671.
58. Schneider, U., et al., *Global Precipitation Analysis Products of the GPCC*. 2011: Deutscher Wetterdienst, Offenbach a. M., Germany.
59. Schneider, U., et al., *Evaluating the Hydrological Cycle over Land Using the Newly-Corrected Precipitation Climatology from the Global Precipitation Climatology Centre (GPCC).* Atmosphere, 2017. **8**(3).
60. CRU, *Climate Research Unite Data*. 2015.
61. Osborn, T.J., *A user guide for ClimGen: a flexible tool for generating monthly climate data sets and scenarios*, in *ClimGen version 1-02*. 2009, Climatic Research Unit (CRU): School of Environmental Sciences, University of East Anglia, Norwich NR4 7TJ, UK. p. 1-17.
62. Finger, P., et al., *GPCC Interpolation Test Dataset at 1.0°*. 2015, Global Precipitation Climatology Centre (GPCC) at Deutscher Wetterdienst.
63. Beguería, S. and S. Vicente, *SPEIbase v.2.6 [Dataset].* 2020.
64. Zhong, R., et al., *scPDSI: Calculation of the Conventional and Self-Calibrating Palmer Drought Severity Index*. 2018.
65. Beguería, S. and S. Vicente, *SPI Calculator*. 2009.
66. Rigby, R.A. and D.M. Stasinopoulos, *Generalized additive models for location, scale and shape.* Journal of the Royal Statistical Society, 2005. **54**: p. 507-554.
67. Akantziliotou, C., R. Rigby, and D. Stasinopoulos. *The R implementation of generalized additive models for location, scale and shape*. in *Statistical modelling in Society: Proceedings of the 17th International Workshop on statistical modelling*. 2002. Statistical Modelling Society.
68. Stasinopoulos, D.M. and R.A. Rigby, *Generalized additive models for location scale and shape (GAMLSS) in R.* Journal of Statistical Software, 2007. **10**: p. 1-46.

 doi:10.20944/preprints202101.0357.v1

69. Stasinopoulos, M., et al., *gamlss: Generalised Additive Models for Location Scale and Shape*. 2020.
70. Hyndman, et al., *forecast: Forecasting Functions for Time Series and Linear Models*. 2020.
71. Scanlon, B.R., et al., *Global evaluation of new GRACE mascon products for hydrologic applications.* Water Resources Research, 2016. **52**(12): p. 9412-9429.
72. Tiwari, V.M., J. Wahr, and S. Swenson, *Dwindling groundwater resources in northern India, from satellite gravity observations.* Geophysical Research Letters, 2009. **36**(18).
73. Rodionov, S.N., *Use of prewhitening in climate regime shift detection.* Geophysical Research Letters, 2006. **33**(12).
74. FAO, *AQUASTAT - FAO's Information System on Water and Agriculture.* 2016.
75. Wilkinson, T., *The Nile: A Journey Downriver Through Egypt's Past and Present*. 2014: Knopf Doubleday Publishing Group. 347.